Advanced Analysis of Corroded Solar Reflectors

Francisco Buendía-Martínez [1], **Aránzazu Fernández-García [1],***, **Florian Sutter [2]**,
Loreto Valenzuela [1] and **Alejandro García-Segura [1]**

[1] CIEMAT-Plataforma Solar de Almería, Ctra. Senés, 04200 Tabernas, Spain;
    francisco.buendia@psa.es (F.B.-M.); loreto.valenzuela@psa.es (L.V.); alexgarsek@gmail.com (A.G.-S.)
[2] German Aerospace Center (DLR), Ctra. Senés, 04200 Tabernas, Spain; florian.sutter@dlr.de
* Correspondence: arantxa.fernandez@psa.es; Tel.: +34-950-387-950

Abstract: The corrosion of the reflective layer is one of the main degradation mechanisms of solar reflectors. However, the appropriate assessment of the corroded reflector samples is not accomplished by the current analysis techniques. On the one hand, the reflectance measurement protocol of non-damaged solar reflectors for concentrating solar thermal technologies is widely addressed in the SolarPACES reflectance guideline. However, this methodology is not adequate for reflectors whose surface is partially corroded by many kind of corrosion agents. In this work, a new measurement technique to properly assess corroded samples was developed. To check the usefulness of the method, several damaged samples (subjected to two accelerated aging tests) were evaluated with the conventional technique and with the improved one. The results showed that a significant discrepancy is observed between the two methods for heavily corroded samples, with average reflectance differences of 0.053 ppt. The visualization of the reflector images illustrated that the improved method is more reliable. On the other hand, both the corrosion products formed and the corrosion rates were identified after each corrosive test. The chemical atmosphere significantly affects the products formed, whereas the corrosion rates are influenced by the test conditions and the reflector quality.

Keywords: concentrating solar thermal energy; corroded solar reflector; improved measurement method; corrosion product; corrosion rate; monochromatic specular reflectance; solar hemispherical reflectance

1. Introduction

The increase of the greenhouse gases in recent years, especially the CO_2 emissions [1], has led to a change in the energy mix [2,3]. The traditional energy sources such as coal, oil, and natural gas are being replaced by other sources with a less aggressive impact on the environment. This change is led by renewables energies [4,5]. Within them the importance of the solar energy should be noted as the best alternative to mitigate the effects originated by the fossil sources because its repercussion on the environment is almost negligible [6–8]. For this reason, solar energy has experienced the renewable energies supply highest average annual growth rate in the world (56.9%), from 1990 to 2015 [9]. Solar energy can be classified into solar thermal energy (STE) or photovoltaic (PV) energy, depending on the energy conversion process. In addition, STE can be divided, depending on the concentration, into concentrating solar thermal (CST) or non-concentrating solar thermal technologies. Regarding CST energy, the total capacity installed worldwide is 5.5 GW, Spain being the country with the highest contribution, 2.3 GW, i.e., the 42% of the total capacity installed [10,11]. According to the International Energy Agency's (IEA) forecast for 2050 [11], an 11% of the worldwide energy mix will be provided by CST systems.

Reflectors, commonly called mirrors, are a crucial component in CST technologies whose goal is to concentrate the radiation in order to transform solar energy into thermal energy [12]. Depending on the reflective layer, mirrors can be classified into aluminum or silvered reflectors [13]. To achieve suitable operating conditions in CST technologies, a reflector with high efficiency should be installed to reach the maximum plant's output [14].

The optical parameter that correctly quantifies the efficiency of a solar reflector is the reflectance, ρ. The measurement of this parameter is a non-trivial issue because many variables are involved in the reflection process, such as the wavelength, λ, the beam divergence of the incident light source, φ_i, and the incidence angle, θ_i of the incoming solar beam, as well as the acceptance angle, φ, of the receiver or measurement device detector. A group of experts have been working on the proper definition of the reflectance under the framework of SolarPACES Task III, within the IEA. Several agreements reached by this group are collected in a document in which current version is titled "Parameters and method to evaluate reflectance properties of reflector materials for concentrating solar power technology" (hereinafter "SolarPACES Reflectance Guideline") [15]. This document has been used as a reference by the CST community for the last years and it has even been mentioned by the first standard published about solar reflectors' durability testing, the UNE 206016:2018 [16], as the measurement method to assess durability experiments.

The measurement protocol described in this guideline, in order to measure new and clean solar reflectors, has proven to be very accurate and easy-to-use for any laboratory or company equipped with conventional commercial instruments [17,18]. However, the proposed conventional method used to characterize aged and/or soiled reflector samples is insufficient and inaccurate since only some specific spots of the samples are assessed and it does not take into consideration θ_i and φ dependence. Recently, several research works which focused on the characterization of soiled reflectors were published [19–22]. However, the evaluation of aged mirrors is a challenging topic that has only been addressed up to now with a prototype instrument specially developed by DLR for that purpose [23].

The durability of the solar reflectors is one of the most important parameters to consider when a CSP plant is designed [13]. In order to guarantee that the reflector is suitable to maintain its optical properties during the whole lifetime of the plant, several aging tests should be performed to assure the reliability of the material. For this purpose, corrosion tests must be carried out to simulate both the corrosion conditions provoked by salty climates, where the concentration of Cl^- ions are higher than usual, as well as polluted atmosphere originated by industries, where the concentration of harmful gases (such as SO_2, NO_2, or H_2S) is extremely high. These real outdoor conditions significantly affect the lifetime of the solar materials because the reflector layer (normally silver) reacts with the chemical compounds of corrosive environments. Consequently, the analysis of the corrosion parameters is a crucial aspect to be considered in the durability studies.

This paper presents an advanced method to analyze corroded solar reflectors. On the one hand, an improved optical measurement technique that accurately measures aged mirrors degraded due to corrosion mechanisms was developed. This method is based on the use of photographic images, the two commercial instruments normally employed in the conventional method (that is, reflectometers and spectrophotometers), and the application of an innovative measurement protocol. Results obtained from this new technique have highly improved the understanding of the overall efficiency decrease produced along the whole solar reflector's surface due to the corrosion effects. On the other hand, the corrosion products appearing on the samples were identified and related to the chemicals added to each corrosive test, and the influence of the materials quality and the testing conditions were related with both the corrosion rates and the total corroded areas.

2. Materials and Methods

This section includes the description of the optical reflectance parameters normally used to characterize solar reflectors, the reflector materials measured in this study, the durability tests applied

to these reflectors, and the measurement equipment employed. Finally, both the conventional optical measurement technique and the improved technique proposed in this work are presented.

2.1. Reflectance Definitions

The optical parameter to correctly characterize a solar reflector is the solar-weighted near-specular reflectance, $\rho_{s,\varphi}([\lambda_a, \lambda_b], \theta_i, \varphi)$, which is defined as ratio of the radiant flux reflected from a surface in the specular direction (and collected into φ) to that of the incident radiation flux (coming with an angle θ_i and weighted in the range from λ_a to λ_b) [14]. Unfortunately, the employed devices to measure it are lab-prototypes [24–27], which are not commercially available yet. Consequently, solar reflectors are normally assessed by an indirect method based on the combination of the following reflectance values:

- Solar-weighted hemispherical reflectance, $\rho_{s,h}([\lambda_a, \lambda_b], \theta_i, h)$, which is calculated by weighting the hemispherical reflectance spectrum, $\rho_{\lambda,h}$, with the solar direct irradiance, G_b, on the earth surface for each λ_i, according to Equation (1) [28].

$$\rho_{s,h}([\lambda_a, \lambda_b], \theta_i, h) = \frac{\int_{\lambda_a}^{\lambda_b} \rho_{\lambda,h}(\lambda, \theta_i, h) G_b(\lambda) d\lambda}{\int_{\lambda_a}^{\lambda_b} G_b(\lambda) d\lambda} \tag{1}$$

where $\rho_{\lambda,h}$ is the ratio of the incident and emitted energy flux of a surface within the complete hemisphere [14], measured with a spectrophotometer. For European and North American latitudes, typical solar direct irradiance spectra are given by the current standard ASTM G173-03 (air mass AM 1.5) [29].

- Monochromatic near-specular reflectance, $\rho_{\lambda,\varphi}(\lambda, \theta_i, \varphi)$, which is the ratio of incident and emitted energy flux of a surface in the specular direction [14]. It is measured with a reflectometer.
- Monochromatic hemispherical reflectance, $\rho_{\lambda,h}(\lambda, \theta_i, h)$, which is the value of the spectral hemispherical reflectance at the same λ of the $\rho_{\lambda,\varphi}$ measured. It is used to calculate the specularity of the reflectors, that is, the ratio between $\rho_{\lambda,\varphi}$ and $\rho_{\lambda,h}$.

2.2. Materials

Second surface silvered-glass reflectors are the most commonly used materials for CST technologies [30,31]. Consequently, this work is focused on the analysis of this type of solar reflectors. They were composed of a low-iron glass substrate (1–4 mm thickness) coated with a silver reflective layer on the backside (see Figure 1). To protect the silver on the backside, the mirror backing system consists of a copper layer and several protective paints. All the reflector samples analyzed were 100 mm by 100 mm and they featured an original edge, in which the metal layers are completely covered and protected by paint layers (protected edge), and three fractured (or unprotected) edges, in which the cross-section of the metal layers was directly in contact with the corrosive atmospheres. This scheme is a common practice in durability research works [32] to properly study the influence of the weathering agents in both undamaged and pre-damaged edges.

Silvered mirrors were composed on the top by glass or polymer surfaces that protect the silver layer of possible environmental weathering. Then, the reflector layer was covered on the back side by a copper layer and different protective paints which prevent the corrosion penetration. The thickness and composition of these paint layers played an important role in order to determine the durability against the corrosion. Due to environmental reasons, current research efforts are ongoing to reduce or remove the lead content of the paints [33].
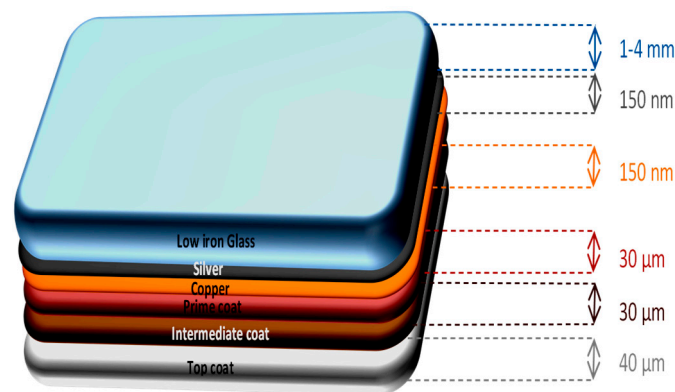
Figure 1. Schematic composition of silvered-glass.

A variety of reflector samples from a number of manufacturers and subjected to two durability tests (Copper-accelerated acetic acid salt spray (CASS) and Kesternich tests, see Section 2.3) were selected for this study, to be analyzed afterwards with the two measurement techniques. All the samples subjected to the CASS test and were labelled with a "C" followed by a number, from one to nine. For the Kesternich tests, the samples were labelled with a "K" followed by a number, from one to nine. Table 1 shows the main characteristics of all the samples tested, including the number and thickness of the back paint layers and the initial reflectance values. Regarding the samples K-1 to K-3, initial damage (a scratch on the paint) was willfully done in order to expose the entire reflector layer to the Kesternich atmosphere [10].

Table 1. Main characteristics of the samples tested.

Sample Code	Number of Protected Edges	Number of Back Paint Layers	Thickness of the Back Paint Layers (μm)	Initial $\rho_{\lambda,\varphi}$ (–)	Initial $\rho_{s,h}$ (–)
C-1	4	3	32-40-30	0.964	0.951
C-2	4	3	32-40-30	0.964	0.951
C-3	4	3	32-40-30	0.964	0.953
C-4	1	2	30-30	0.967	0.955
C-5	1	3	28-35-35	0.961	0.951
C-6	1	3	28-35-35	0.964	0.951
C-7	1	2	30-30	0.966	0.955
C-8	1	3	28-35-35	0.961	0.951
C-9	1	2	30-30	0.965	0.954
K-1	1	3	28-37-37	0.954	0.945
K-2	1	3	28-37-37	0.956	0.944
K-3	1	3	28-37-37	0.956	0.944
K-4	4	3	28-37-37	0.957	0.944
K-5	4	3	28-37-37	0.957	0.943
K-6	4	3	28-37-37	0.958	0.945
K-7	4	3	28-37-37	0.959	0.944
K-8	4	3	28-37-37	0.959	0.945
K-9	4	3	28-37-37	0.958	0.943

2.3. Durability Tests

All the samples included in this study have in common that the main degradation mechanism provoked by the two durability experiments applied (CASS and Kesternich tests) was the corrosion in the reflective silver layer, both in the form of corrosion spots or corrosion penetration through the edges. This is one of the typical degradation effect reported for silvered-glass reflectors [13,34].

On the one hand, CASS test is one of the most common aging experiments applied to simulate corrosion in solar reflectors [13]. In accordance with the ISO 9227 [16], the samples were tested at

a temperature (*T*) of *T* = 50 °C and 100% of relative humidity (*RH*), where an uninterrupted spray composed by a solution of demineralized water, 50 g/L of NaCl and 0.26 g/L of $CuCl_2$ was continuously wetting the samples. The condensation rate obtained for a surface of 80 cm^2 in the testing chamber with these conditions was 1.5 mL/h. Moreover, the pH of the solution was kept between 3.1 and 3.3 and it was adjusted by adding acid or basic compounds such as HCl or CH_3COOH and NaOH. Three CASS were conducted, varying the testing time (which was 330, 430, and 480 h), with the goal of producing several different levels of corrosion.

On the other hand, Kesternich test was utilized to reproduce industrial atmospheres where the concentration of corrosive gases is very high (typically known as acid rain conditions) and consequently the main degradation mechanism is the corrosion of the reflective layer. To simulate such polluted environments, the samples were subjected to two different SO_2 concentrations (3333 and 6667 ppm) and temperatures (*T* = {25, 40, 50} °C) during 8 h and to ambient conditions for 16 h, which suppose a cycle of 24 h in total. As in the previous test, different testing time was applied to vary the severity of the corrosion.

In addition to the testing conditions, the intensity of the corrosion appearing in the different samples tested depended on the number, the thickness, and the composition of the back coating layers (see Table 1). Table 2 presents a summary of the testing conditions corresponding to the different experiments applied.

Table 2. Tests conditions of the experiments applied to the studied reflector samples.

Sample Code	Durability Test	Testing Conditions	Testing Time (h)
C-1, C-2, C-3		*T* = 50 ± 2 °C, pH = [3.1, 3.3] at 25 °C	480
C-4, C-5, C-6, C-7	CASS	Sprayed NaCl solution of 50 ± 5 g/L and	430
C-8, C-9		0.26 ± 0.02 g/L $CuCl_2$	330
K-1, K-2, K-3		*T* = 40 °C, *RH* = 100% $[SO_2]$ gas = 6667 ppm	910
K-4, K-5, K-6	Kesternich	*T* = 50 °C, *RH* = 100% $[SO_2]$ gas= 3333 ppm	768
K-7, K-8, K-9		*T* = 25 °C, *RH* = 100% $[SO_2]$ gas = 3333 ppm	720

2.4. Analysis Techniques

This section describes the two optical measurement equipment used to measure reflectance in both the conventional and the improved techniques.

2.4.1. Reflectometer

The equipment selected to measure $\rho_{\lambda,\varphi}$, was the portable specular reflectometer 15R-USB by Devices and Services (D&S, Dallas, TX, USA) [35], which was specifically developed by the company in cooperation with Sandia National Laboratories to assess solar reflectors [36] (see Figure 2). It has a light-emitting diode (LED) source of λ = [635, 685] nm, with a peak at λ = 660 nm. φ can be selected from φ = {3.5, 7.5, 12.5, 23.0} mrad, and the θ$_i$ = 15°. The instrument produces a collimated beam to a diameter of 10 mm (which corresponds to the measurement spot size) so that all of the reflected beam can be collected by the 22 mm diameter receiver lens. The beam deviation of the collimated incident beam is φ$_i$ = 5 mrad and therefore almost matching the sun disc on a clear-sky day. The instrument allows measuring curved mirrors and also first and second surface mirrors with different top-layer thickness.

Figure 2. Portable specular reflectometer 15R-USB by Devices and Services (D&S).

All the measurements were taken at φ = 12.5 mrad. The instrument used (serial number 117) has a repeatability of ±0.002 and a resolution of ±0.001. The calibrated reference standard, a 4-mm second-surface silvered-glass sample by OMT (serial number OMT-214044-02), has an uncertainty of 0.0015. Considering these values, the expanded type B uncertainty is 0.006. All measurements were taken in steady conditions (at constant temperature) by the same technician.

2.4.2. Spectrophotometer

The scanning spectrophotometer (model Lambda 1050, Perkin Elmer (PE), Waltham, MA, USA) with a 150-mm diameter integrating-sphere accessory was employed to measure $\rho_{\lambda,h}$ (see Figure 3) [37]. It is a UV/Vis/NIR double beam and double monochromator instrument with two light sources, a deuterium lamp for the UV range, and a halogen lamp for the Vis/NIR range. The beam source has a spectral λ range from 175 to 3300 nm, θ_i = 8° and is about 17 mm by 9 mm size. The detection system is composed of a photomultiplier for the UV/Vis range, and two detectors (a Peltier controlled PbS detector and a InGaAs detector) for the NIR range. The measurement spot in this case is 9 mm by 17 mm.

Figure 3. Spectrophotometer Lambda 1050 by Perkin Elmer (PE).

Measurements were taken in 5 nm steps in the range λ = [320, 2500] nm. The maximum response time (0.04 s) was selected in the whole λ range, except in λ = [600, 880] nm, where the minimum response time (1 s) was chosen. This combined response time was selected because it presents a proper compromise between accuracy and measuring time. The instrument used (serial number 1050N9061802) has an accuracy of ±0.007 (at 635 nm). The calibrated reference standard, a 4-mm second-surface silvered-glass sample by OMT (serial number OMT-214044-02), has an uncertainty of

0.0015. Considering these values, the expanded type B uncertainty is 0.016. All measurements were taken in steady conditions (at constant temperature and with an opaque cover) by the same technician.

2.4.3. EDX

Energy dispersive X-ray analysis (EDX) is a technique that uses X-ray to identify the elemental composition of a material. In our case, a QUANTAX EDS system (Bruker, Durham, UK) was utilized to perform the analysis. This EDX system is coupled to a scanning electron microscopy (SEM), model S-3400N (Hitachi, Tokyo, Japan) that generates a microscopic image that is scanned by the EDX system. The results provided by the EDX analysis consist of spectra which exhibit peaks corresponding to the elemental composition of the sample analyzed.

2.5. Conventional Reflectance Measurement Technique

The conventional method applied is in agreement with the current version of the "SolarPACES Reflectance Guideline" [15], which has been extensively employed to characterized solar reflectors in durability studies [37–39]. According to it, the following parameters must be measured to monitor the aging of solar reflectors:

- $\rho_{s,h}$ at $\theta_i \leq 15°$ and in the range $\lambda = [320, 2500]$ nm.
- $\rho_{\lambda,\varphi}$ at one defined λ in the range $\lambda = [400, 700]$ nm, $\theta_i \leq 15°$, and a φ in the range of $\varphi = [0, 20]$ mrad.
- $\rho_{\lambda,h}$ at the same λ as for $\rho_{\lambda,\varphi}$ to calculate the specularity of the reflector samples.

As it is recommended in this guideline, $\rho_{\lambda,\varphi}$ was measured in five points of each reflector sample, taken in the center of the sample and close to the four corners of the sample (see Figure 4), and the average value as well as the standard deviation was reported. The measurements were always taken at a distance to the sample edge higher than 10 mm. The equipment used for the measurements was the portable specular reflectometer 15R-USB by D&S, described in Section 2.4.1. A mask was always used to characterize each reflector sample in order to always measure the same spots and so properly assess the evolution of the possible corrosion partners.
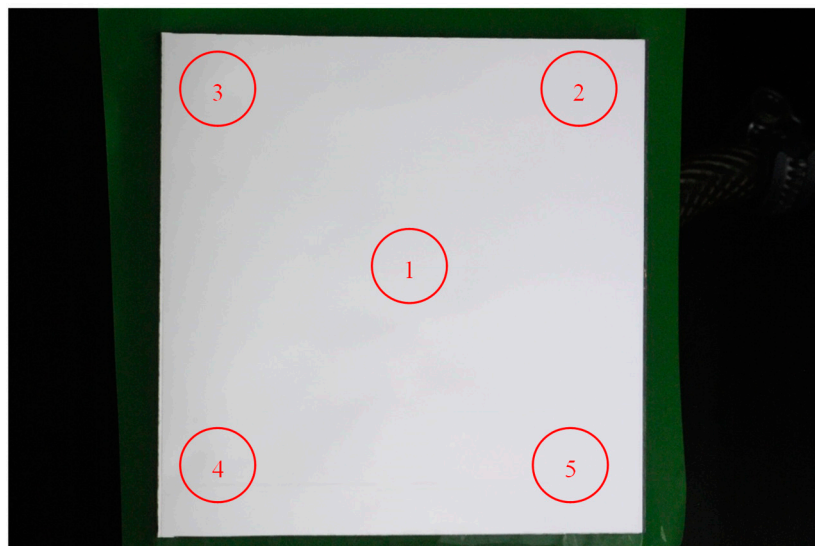

Figure 4. Five spots measured on each reflector sample with the reflectometer, according to the conventional measurement technique.

In addition, $\rho_{s,h}$ measurements were taken at the center of the reflector samples and repeated at the same point thrice (rotating the sample 0°—no rotation—, 90°, and 180°) to check any possible anisotropy. Due to the shape of the beam spot and the possible inaccuracy in the positing after the

rotation, the three measurement spots might not be exactly the same (see Figure 5). Again, both the average value and the standard deviation were reported. The equipment used for the measurements was the spectrophotometer Lambda 1050 by PE, described in Section 2.4.2.
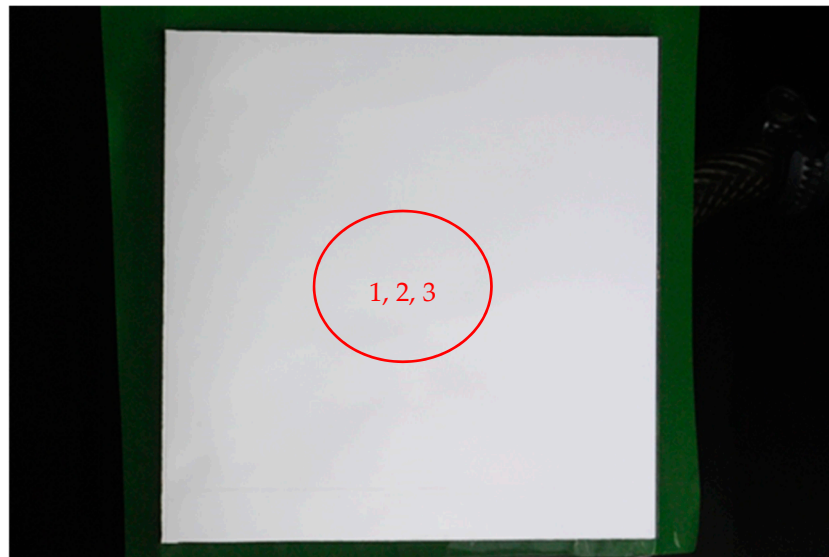

Figure 5. Three spots measured on each reflector sample with the spectrophotometer, according to the conventional measurement technique.

As it has been stated, with this method the spots monitored are always the same and consequently it is impossible to distinguish between measurements taken in corroded and non-corroded areas. This fact can cause misunderstanding and errors in the average reflectance of the whole reflector sample because in a reflector whose corroded area is almost negligible, this small degraded area might coincide with the measurement spot and consequently the reflectance would decrease drastically in an unfair manner. Also, the opposite event could happen, in a reflector sample whose useful surface is quite small because the corrosion affects most of the surface, the measurement spot could coincide with a non-corroded area and the reflectance would be much higher than the real one. For this reason, in many occasions the results achieved with this method are not representative of the average reflectance of the whole reflector sample.

2.6. Improved Reflectance Measurement Technique

An improved reflectance measurement technique was developed in this study to obtain more representative results by taking into consideration the portion of the total reflector area, A_T, affected by the corrosion. Following this goal, this method is based on distinguishing the corroded area, A_C, and the useful (non-corroded) area, A_{NC}, of the reflector sample, and weighting the average reflectance of each area accordingly, as indicated in Equation (2) for the weighted monochromatic specular reflectance, $\rho_{\lambda,\varphi,w}$, and Equation (3) for the weighted solar hemispherical reflectance, $\rho_{s,h,w}$.

$$\rho_{\lambda,\varphi,w} = \frac{A_{NC}}{A_T} \times \rho_{\lambda,\varphi,NC} + \frac{A_C}{A_T} \times \rho_{\lambda,\varphi,C} \tag{2}$$

$$\rho_{s,h,w} = \frac{A_{NC}}{A_T} \times \rho_{s,h,NC} + \frac{A_C}{A_T} \times \rho_{s,h,C} \tag{3}$$

where the subscripts "*NC*" and "*C*" in the reflectance mean non-corroded and corroded, respectively. To calculate the weighted reflectance, the first step consists in taking an image of the sample to determine A_C and A_{NC}.

In Figure 6, it is depicted the histogram with the different tonalities of black and white that could exist in the pixels (from zero to 255). Depending on the threshold chosen, the detection of black and white can vary. If the threshold selected is zero, all the pixels colors will be detected as white, while if it is 255, the opposite case would occur, and all the pixels will be detected as black. The Figure 6a shows the histogram of a sample with black corrosion. In this case, the white tonalities started in the range of 188 to 232 and the black from 58 to 125. The threshold selected was 148, distinguishing perfectly between corroded (from zero to 148) and non-corroded area (from 148 to 255). However, for samples where the corrosion appears with a color different to black, the threshold should be modified in order to detect this corrosion (see Figure 6b). In this case, the corrosion tonalities are yellow and the threshold selected to recognize this color as corrosion was 194. As a consequence, the corroded area was counted from zero to 194.
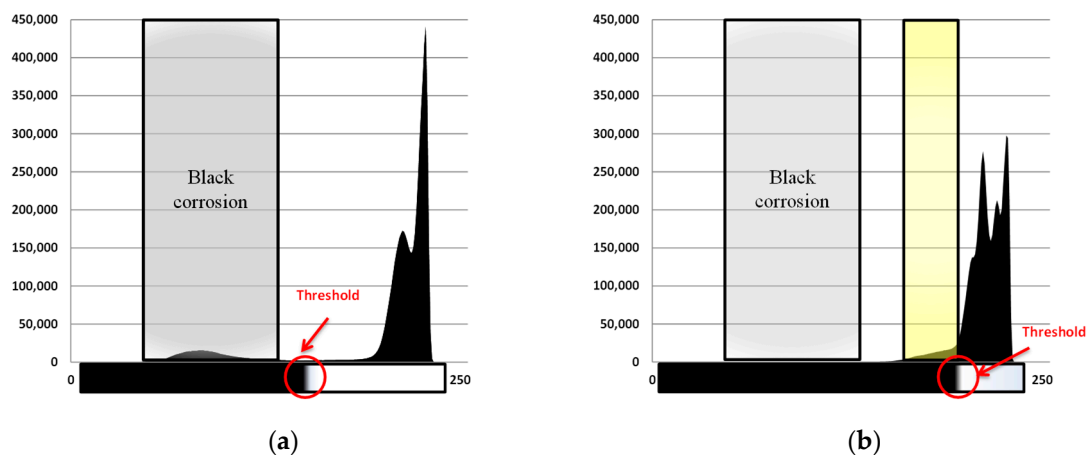

(**a**)   (**b**)

Figure 6. Histogram image of a corroded sample with black corrosion (**a**) and yellow corrosion (**b**).

The pictures were taken with a homogenous illumination of 1000 mA in the whole sample to avoid shadow areas and with an exposure time of 1/15 s. As it was previously explained, for typical corrosion whose corrosion color is black, the threshold employed was 148. Nevertheless, for corrosion whose color is not black, for instance yellow, the threshold should be changed to higher values in order to detect the degradation. Additionally, a distinction between the corroded area starting in the cut edges and originated by corrosion spots can be implemented. With an image treatment software (Matlab or ImageJ), it is possible to perform the transformation of the real image to a binary image, where the corroded surface is in black and the useful area is in white, permitting to estimate the no-corroded surface percentage (see Figure 7). After several tests, it was determined that the minimum quality recommended to take the image should be 254.6 pixels/mm, which corresponds to a vertical and horizontal resolution of 300 ppi. The accuracy of the software is good enough because the operator of the software can avoid manually the side effects that could be interpreted as corrosion but they are not. Examples of this kind of side effects are shading when the photo was taken, and soiling deposited on the reflector surface. Consequently, the accuracy in detecting the real corrosion is very high. To have a quantitative value of this accuracy, one corroded reflector sample was analyzed by taken five pictures and calculating the corroded area with the software, keeping all the parameters constant. The repeatability obtained was ±0.07%.

Figure 7. Binary image of Figure 8 to calculate the total corroded area.
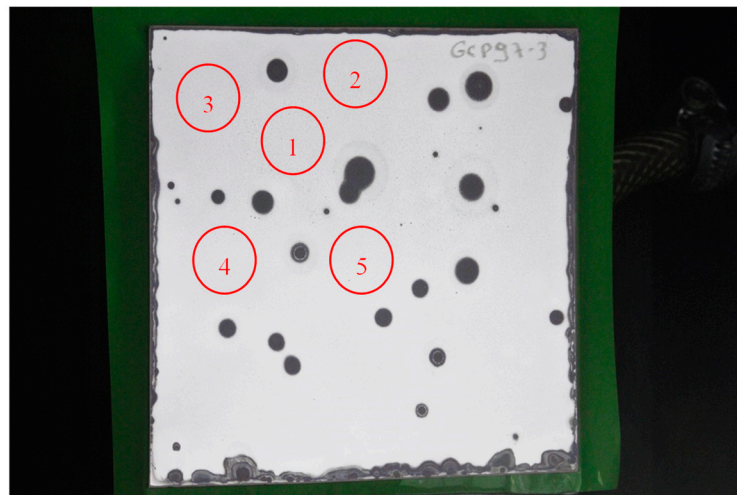

Figure 8. Five measurements taken along the non-corroded surface of a partially corroded reflector.

The second step is based on taking the reflectance measurements in the useful area to calculate $\rho_{\lambda,\varphi,NC}$ or $\rho_{s,h,NC}$. On the one hand, for corrosion with a dark color, the reflectance of the corroded area can be approximated to zero (black surface), $\rho_{\lambda,\varphi,C} = \rho_{s,h,C} = 0$. Then, for the calculation of $\rho_{\lambda,\varphi,NC}$ with the reflectometer, five measurements are randomly taken along the non-corroded reflector surface. In samples where the corrosion is heterogeneous, special care must be taken to avoid measuring in corrosion spots and in the corroded edges (see Figures 8–10). On the other hand, if the corrosion is not dark (for instance, yellow), it is necessary to measure, as a minimum, once in the corroded area to calculate the $\rho_{\lambda,\varphi,C}$ or $\rho_{s,h,C}$ and to change the threshold value for taking into consideration this area (see Figure 10). The same rules should be followed to calculate $\rho_{s,h,NC}$ with the spectrometer, with the only exception that in this case only three measurements are recommended to avoid a very time consuming process.
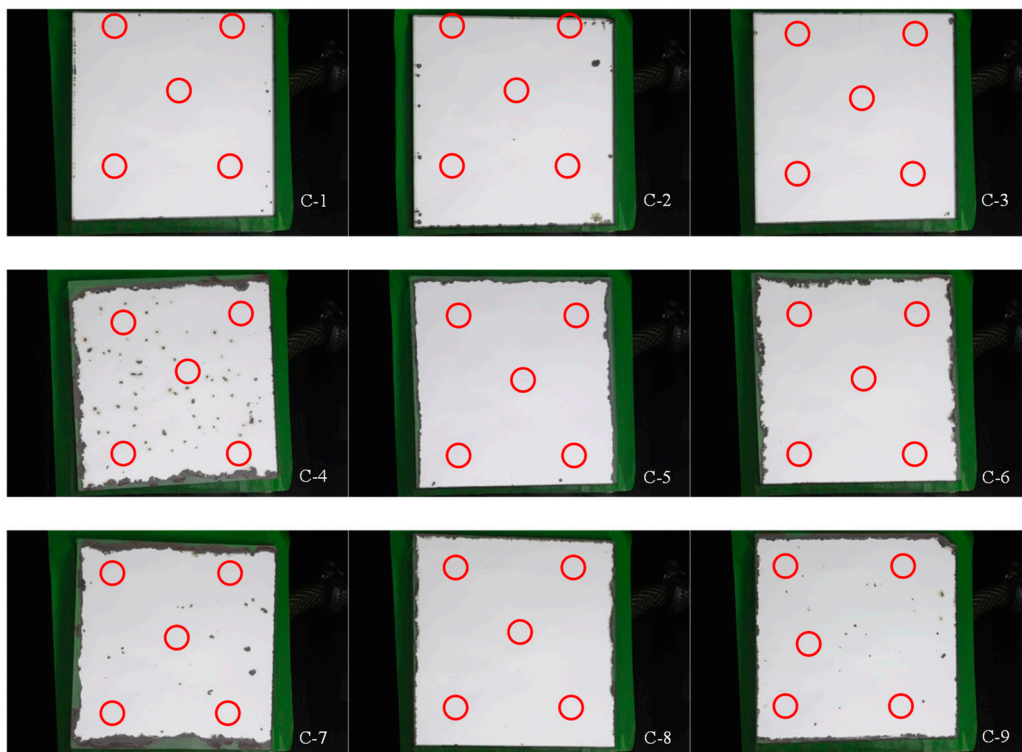
Figure 9. Images of the corroded reflector samples aged in the CASS test, with the measurement spots marked with red circles.

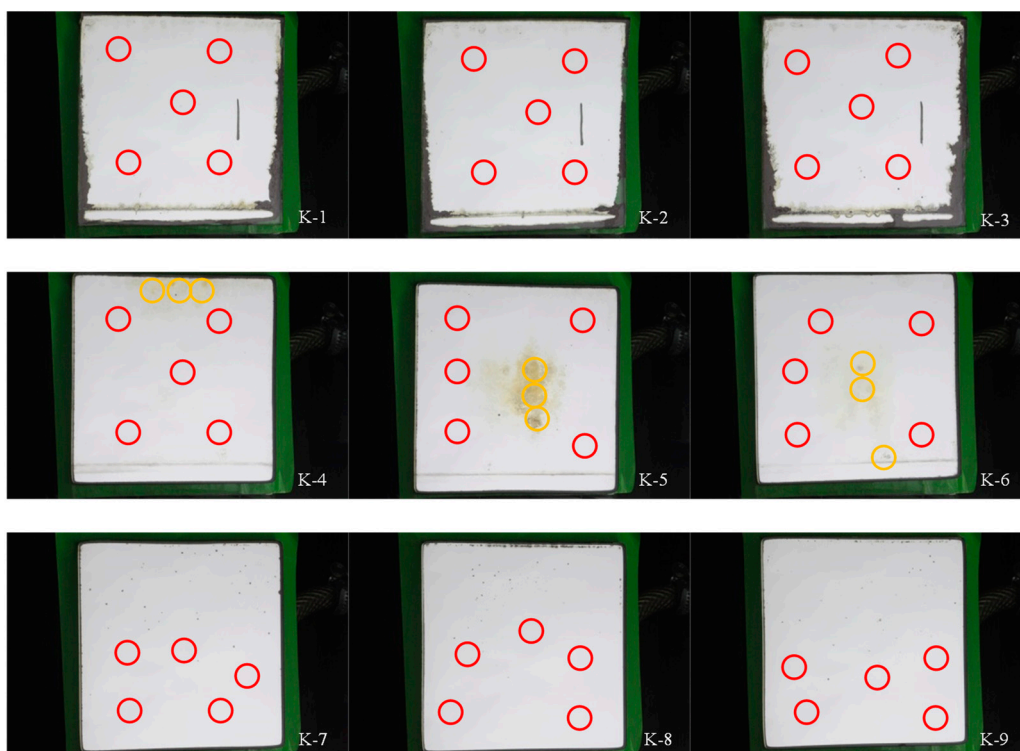**Figure 10.** Images of the corroded reflector samples tested in the Kesternich test, with the measurement spots marked with red circles (non-corroded area) or yellow circles (corroded area).

3. Results and Discussion

This section sets out results of the corrosion products formed, the corrosion rate and the reflectance (both average and standard deviation values) of corroded samples measured with the two different

measurement techniques. For purposes of clarity, the results are divided into two subsections according to the accelerated aging test used to corrode the reflectors. Moreover, images of these reflector samples are provided to show the different corrosion levels and the points where $\rho_{\lambda,\varphi,C}$ (in yellow) and $\rho_{\lambda,\varphi,NC}$ (in red) were measured.

3.1. Reflectance Analysis

3.1.1. CASS Test

Table 3 presents the average and standard deviation of $\rho_{\lambda,\varphi}$, $\rho_{\lambda,\varphi,NC}$, $\rho_{s,h}$, and $\rho_{s,h,NC}$ of the corroded samples using both measurement techniques and after several testing times in the CASS test (see Table 2 for the testing conditions).The values of $\rho_{\lambda,\varphi,w}$ and $\rho_{s,h,w}$ are calculated through the Equations (1) and (2), weighting the $\rho_{\lambda,\varphi,NC}$ and $\rho_{s,h,NC}$ with the corroded area, as also shown in the table. The weighted reflectance value obtained with the improved measurement technique and the reflectance measured with the conventional method are both in bold for an easy comparison of the results (see the Discussion section). Furthermore, the corresponding images of these samples are illustrated in Figure 9.

Table 3. Results of the corroded area and the monochromatic specular and solar hemispherical reflectance values for both reflectance measurement techniques, applied to the corroded samples aged in the CASS test.

Sample Code	Corroded Area (%)	Monochromatic Specular Reflectance						Solar Hemispherical Reflectance					
		Conventional Reflectance Method		Improved Reflectance Method				Conventional Reflectance Method		Improved Reflectance Method			
		$\rho_{\lambda,\varphi}$ (–)		$\rho_{\lambda,\varphi,NC}$ (–)		$\rho_{\lambda,\varphi,w}$ (–)		$\rho_{s,h}$ (–)		$\rho_{s,h,NC}$ (–)		$\rho_{s,h,w}$ (–)	
		$\overline{X}$	σ	$\overline{X}$	σ	$\overline{X}$	σ	$\overline{X}$	σ	$\overline{X}$	σ	$\overline{X}$	σ
C-1	0.30	**0.964**	0.001	0.963	0.001	**0.960**	0.001	**0.950**	0.000	0.951	0.001	**0.948**	0.001
C-2	1.42	**0.963**	0.001	0.962	0.000	**0.949**	0.000	**0.949**	0.004	0.951	0.000	**0.937**	0.000
C-3	0.11	**0.964**	0.001	0.964	0.001	**0.963**	0.001	**0.952**	0.000	0.952	0.000	**0.951**	0.000
C-4	13.00	**0.921**	0.040	0.945	0.012	**0.822**	0.010	**0.931**	0.008	0.935	0.007	**0.813**	0.006
C-5	7.72	**0.960**	0.002	0.959	0.000	**0.886**	0.000	**0.951**	0.000	0.951	0.000	**0.878**	0.000
C-6	9.45	**0.963**	0.001	0.964	0.000	**0.873**	0.000	**0.951**	0.002	0.951	0.001	**0.861**	0.001
C-7	15.00	**0.963**	0.001	0.963	0.000	**0.819**	0.000	**0.950**	0.001	0.951	0.000	**0.808**	0.000
C-8	3.80	**0.959**	0.003	0.959	0.002	**0.922**	0.002	**0.949**	0.000	0.949	0.000	**0.913**	0.000
C-9	7.00	**0.959**	0.003	0.964	0.001	**0.892**	0.001	**0.943**	0.000	0.949	0.000	**0.883**	0.000

3.1.2. Kesternich Test

Regarding the samples subjected to the Kesternich test (see Table 2 for the testing conditions), Table 4 presents the average and standard deviation of $\rho_{\lambda,\varphi}$, $\rho_{\lambda,\varphi,NC}$, $\rho_{s,h}$, and $\rho_{s,h,NC}$ for the measurements using both measurement techniques after several times in three Kesternich tests at different gas concentration and temperature values (see Table 2 for the specific testing conditions). For the material K-4, K-5, and K-6, the $\rho_{\lambda,\varphi,C}$ obtained was 0.85, 0.32, and 0.86 ppt and the $\rho_{s,h,C}$ was 0.87, 0.82, and 0.87 ppt, respectively. $\rho_{\lambda,\varphi,C}$ and $\rho_{s,h,C}$ for the rest of the samples were zero. Also, the corroded area is presented in this table to calculate the weighted reflectance ($\rho_{\lambda,\varphi,w}$ and $\rho_{s,h,w}$) with the improved method. As in Table 3, final reflectance values of both methods are shown in bold. In addition, Figure 10 exhibits representative images of the corroded samples after the Kesternich test.

Table 4. Results of the corroded area and the monochromatic specular and solar hemispherical reflectance values for both reflectance measurement techniques, applied to the corroded samples aged in the Kerternich test.

Sample Code	Corroded Area (%)	Monochromatic Specular Reflectance						Solar Hemispherical Reflectance					
		Conventional Reflectance Method		Improved Reflectance Method				Conventional Reflectance Method		Improved Reflectance Method			
		$\rho_{\lambda,\varphi}$ (–)		$\rho_{\lambda,\varphi,NC}$ (–)		$\rho_{\lambda,\varphi,w}$ (–)		$\rho_{s,h}$ (–)		$\rho_{s,h,NC}$ (–)		$\rho_{s,h,w}$ (–)	
		$\overline{X}$	σ	$\overline{X}$	σ	$\overline{X}$	σ	$\overline{X}$	σ	$\overline{X}$	σ	$\overline{X}$	σ
K-1	9.00	**0.954**	0.001	0.954	0.001	**0.869**	0.001	**0.945**	0.000	0.943	0.000	**0.858**	0.000
K-2	9.58	**0.951**	0.003	0.953	0.001	**0.862**	0.001	**0.944**	0.000	0.942	0.000	**0.852**	0.000
K-3	12.78	**0.954**	0.002	0.955	0.001	**0.833**	0.001	**0.944**	0.001	0.942	0.000	**0.822**	0.000
K-4	4.32	**0.955**	0.003	0.957	0.002	**0.952**	0.002	**0.944**	0.000	0.941	0.001	**0.938**	0.001
K-5	8.82	**0.778**	0.300	0.932	0.030	**0.879**	0.027	**0.782**	0.020	0.939	0.004	**0.929**	0.004
K-6	7.02	**0.929**	0.040	0.960	0.003	**0.953**	0.003	**0.887**	0.010	0.943	0.002	**0.938**	0.002
K-7	0.37	**0.954**	0.002	0.957	0.001	**0.953**	0.001	**0.945**	0.000	0.945	0.000	**0.942**	0.000
K-8	0.95	**0.954**	0.002	0.955	0.001	**0.946**	0.001	**0.944**	0.000	0.945	0.000	**0.936**	0.000
K-9	0.43	**0.954**	0.001	0.956	0.000	**0.951**	0.000	**0.942**	0.001	0.944	0.000	**0.940**	0.000

3.1.3. Discussion of the Measurement Techniques

As can be seen in the Tables 3 and 4, the reflectance results of both measurement techniques are quite different. Usually, the conventional method provides much higher reflectance values than the improved method because the corroded area of the sample is not properly considered.

On the one hand, if $\rho_{\lambda,\varphi}$ and $\rho_{\lambda,\varphi,NC}$ are compared to $\rho_{s,h}$ and $\rho_{s,h,NC}$, the values are quite similar for most of the cases (with differences below the type B uncertainty of the equipment) because the probability of measuring in non-corroded area with the conventional method is high, due to the low portion of corroded area (not greater than the 15% of the total area), as can be observed in the tables and pictures. However, given that the conventional method always measures in the same spots, there is a chance that the corrosion may appear in the measurement area. For instance, this event occurs in samples C-4 and K-5 for the monochromatic specular reflectance (where the measurement spots are distributed in the whole surface, see Figure 4), and K-5 and K-6 for the solar hemispherical reflectance (where the measurements spots are located in the central area, see Figure 5). This fact also provokes an increase in the standard deviation (reaching values up to 0.300). Additionally, the $\rho_{\lambda,\varphi,NC}$ and $\rho_{s,h,NC}$ assess the quality of the mirror surface which is not corroded, providing a more reliable reflectance average because uncertainty related to the corroded area is reduced. Thus, with these parameters ($\rho_{\lambda,\varphi,NC}$ and $\rho_{s,h,NC}$) it is possible to evaluate the quality of the reflector layer.

On the other hand, a great discrepancy between $\rho_{\lambda,\varphi}$ and $\rho_{\lambda,\varphi,w}$, and $\rho_{s,h}$ and $\rho_{s,h,w}$ exists for most of the reflectors, where the improved measurement technique provides smaller reflectance results because the corroded area is taken into consideration. To quantify the importance of this discrepancy, the reflectance differences between the conventional and the improved methods, $\rho_{\lambda,\varphi}$-$\rho_{\lambda,\varphi,w}$ and $\rho_{s,h}$-$\rho_{s,h,w}$, are calculated (for all samples except K-5 and K-6). As a result, the average values achieved are 0.053 ppt for both the monochromatic specular and solar hemispherical reflectance. Especially, the samples C-4, C-6, C-7 (Table 3), and K-3 (Table 4) show significant monochromatic specular reflectance discrepancies, where the maximum difference of 0.144 ppt is reached for the sample C-7. Regarding the solar hemispherical reflectance, a maximum reflectance discrepancy of 0.142 ppt between both methods is achieved for the sample C-7. This fact occurs because these specific samples are very damaged, as it is depicted in the Figures 9 and 10. Consequently, the measurements taken with the conventional method only were taken in the non-corroded area, obtaining a reflectance value much higher than the real. Otherwise, the opposite case occurs for the samples K-5 and K-6 where the monochromatic specular and solar hemispherical reflectance in the improved method is 0.101, 0.024 and 0.147, 0.051 ppt higher than in the conventional one, respectively. This difference is induced by a coincidence

between the measurement spots of the conventional method and the corroded area, provoking an excessive decrease of the reflectance.

Finally, there are two cases that are worth mentioning (C-7 and K-3), where the main corrosion is suffered in the edges of the reflector samples. In both cases, the corroded area is very high but the two types of measured reflectance ($\rho_{\lambda,\varphi}$ and $\rho_{\lambda,\varphi,NC}$ and $\rho_{s,h}$ and $\rho_{s,h,NC}$) show unrealistically high values. However, the weighted reflectance ($\rho_{\lambda,\varphi,w}$ and $\rho_{s,h,w}$) do present low values, which are more reliable because the corrosion mainly appeared in areas not accessible for the measurement instruments (the edges).

3.2. Corrosion Products Formed and Corrosion Rates

This section presents all the results of the advanced analysis performed in the corroded samples in order to determine the corrosion rates and the corrosion products appeared after the accelerated aging tests. It is divided into two sections, according to the accelerated aging tests.

3.2.1. CASS Test

As depicted in Figure 9, the corrosion of the samples in the CASS test was provoked by two different degradation mechanisms, which are the occurrence of corrosion spots and the corrosion along the edges. In order to determine the corrosion products that might appear in both types of degradation defects, an EDX analysis was performed in the silver layer of a reflector sample in the initial status and also in a corrosion defect of a reflector sample after being subjected to the CASS test during 480 h. For both types of degradation defects, the formation of oxides and chlorides of silver was observed (see Figure 11). This originates the appearance of new compounds whose reflectance is zero, subsequently reducing the optical properties of the reflectors. As can be seen, the EDX analysis before the CASS test did not detect the presence of Cl^- ions in the composition of the silver layer (see Figure 11a). However, after 480 h of the CASS test, a new peak appeared in the spectrum, which corresponds to Cl^- ion (see Figure 11b). The presence of silicon, magnesium, and sodium is due to the proximity of the glass to the measured zone. In addition, copper is detected because this layer is deposited on the back side of the silver layer for protection. Lastly, the non-identified peaks correspond to the gold which was sputtered on the sample to improve the quality of the EDX analysis.

Another important parameter to assess the corrosion detected in the samples is the corrosion rate (see Table 5), which is calculated as the corroded area divided by the testing time. This parameter varied in function of the test severity (see Table 2), the number of protected edges and the types of paints of the reflector (see Table 1).

Table 5. Corrosion rates of samples tested in the CASS test.

Sample Code	C-1	C-2	C-3	C-4	C-5	C-6	C-7	C-8	C-9
Corrosion Rate (cm^2/h)	0.0006	0.003	0.0002	0.0300	0.0220	0.0200	0.0500	0.012	0.0210

The main conclusions obtained from the corrosion rates are:

- The protection of the edges is essential to improve the durability of a reflector. As it is shown in the Table 5, the samples tested during the longest time obtained the lowest corrosion rate because all of the edges were protected.
- As for the number of paint layers, the samples C-4, C-5, C-6, and C-7 were tested during the same time (430 h). However, a great difference is observed among their corrosion rates, being higher for samples C-4 and C-7, which contain two paint layers instead of three. The same argument is used for samples tested during 330 h, where C-9 (two paint layers) has a corrosion rate twice as high as C-8 (three paint layers).
- Another parameter to consider in the evaluation of the corrosion rate is the testing time. As can be seen for samples with only one protected edge and the same number of paint layers, the corrosion

rate increases with time. For example, this is the case of C-4 and C-7 against C-9 (both with two paint layers), where C-7 has higher corrosion rate due to the longer testing time.
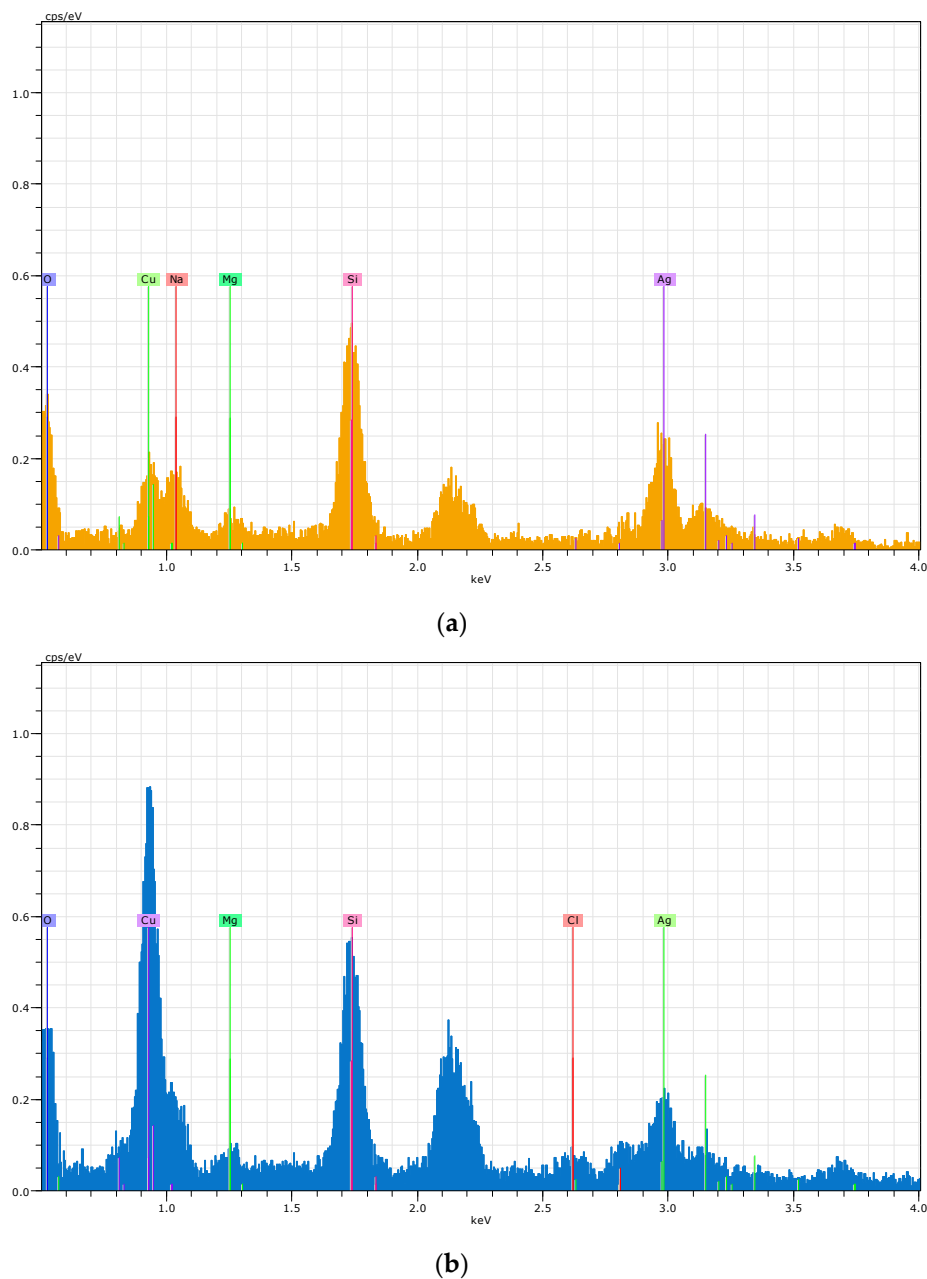

(**a**)

(**b**)

Figure 11. Energy dispersive X-ray analysis (EDX) analysis of the reflector silver layer before (**a**) and after of 480 h (**b**) of the CASS test.

It is also important to highlight that these conclusions can be also extrapolated to the differences detected in the corroded area (see Table 3) because, as expected, a perfect match was found between both parameters (corroded area and corrosion rate).

3.2.2. Kesternich Test

As was previously reported for the CASS test, the main corrosion mechanisms are the appearance of corrosion spots and edge corrosion. To characterize the products formed in the corrosion process, an EDX analysis of a sample tested during 910 h in a Kesternich test was carried out. It was observed that the silver layer was significantly affected by the SO_2 atmosphere, due to the reaction of the silver with

the sulfur, and provoking the appearance of new compounds. As illustrated in Figure 12, the emergence of sulfur is detected, as well as other compounds such as silicon, gold, and sodium (aforementioned and explained in Section 3.2.1). Another remarkable result is the absence of copper in this analysis, probably due to a total corrosion of the copper layer by the sulfurous atmosphere.
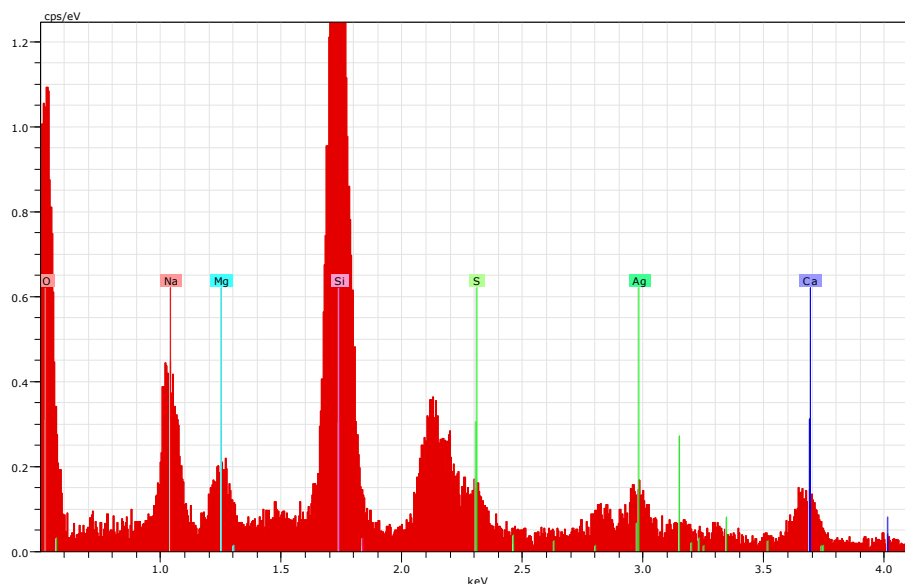

Figure 12. EDX analysis of the reflector silver layer after of 910 h of Kesternich test.

In addition, the corrosion rates of all the samples tested in the Kesternich test were obtained (see Table 6). The method to calculate this parameter was already described in Section 3.1.

Table 6. Corrosion rates of samples tested in the Kesternich test.

Sample Code	K-1	K-2	K-3	K-4	K-5	K-6	K-7	K-8	K-9
Corrosion Rate (cm^2/h)	0.010	0.010	0.014	0.005	0.010	0.009	0.001	0.001	0.001

In this test, the influence of the temperature and the SO_2 concentration must be taken into account, arriving at the following main considerations:

- As it was mentioned in the CASS results, the protection of the edges is a very important issue. This was also noticed in the Kesternich test because the three samples with only one protected edge (K-1, K-2, and K-3) showed the highest corrosion rates.
- With respect to the gas concentration, it was also noticed that the degradation is increased at the highest SO_2 concentration (samples K-1, K-2, and K-3).
- Finally, the influence of the testing temperature can be analyzed by comparing samples tested at the same SO_2 concentration (3333 ppm) but at different temperatures, i.e., samples K-4, K-5, and K-6 (tested at 50 °C) against samples K-7, K-8, and K-9 (tested at 25 °C). As can be observed, the corrosion rates are much higher for samples tested at the highest temperature. Consequently, the influence of the temperature is crucial in this test.

As it was already mentioned for the CASS test, these conclusions can be also extrapolated to the differences detected in the corroded area (see Table 4) because, as expected, a perfect match was found between both parameters (corroded area and corrosion rate).

4. Conclusions

The investigation presented in this work demonstrates that the reflectance of corroded reflector samples is not suitably assessed by the conventional measurement technique. Thus, a new methodology

is required to analyze corroded reflectors. Following up on this goal, an improved measurement technique that provides an appropriate reflectance value for corroded samples was developed. This method was able to distinguish between corroded and non-corroded surfaces and to determine a weighted reflectance value. The average differences between both methods are 0.053 ppt for both the monochromatic specular and the solar hemispherical reflectance. Discrepancies of up to 0.144 and 0.147 ppt are reached for monochromatic specular and solar hemispherical reflectance, respectively. As it was demonstrated by image inspection of the reflector samples, the reliability of both monochromatic specular and solar hemispherical reflectance was much higher when the improved method was utilized, even in the cases where the corrosion is mainly found near the sample edges.

Moreover, it was proved that the severity of the corrosion originated in the reflectors depends on several parameters, such as the reflector material quality and the corrosion test conditions. With respect to the reflector material quality, the numbers of back paint layers as well as the number of protected edges are two of the key indicators of reflector resistance against corrosion. In this sense, it was determined that the corrosion rate and the corroded area decrease as the number of both the back paint layers and the protected edges increase. Additionally, the degradation of the reflector samples increases with the severity of the test conditions and the duration of the test.

Regarding the products formed after the aging tests, the EDX analysis of the silver layer shows that chlorine appeared in the CASS test, whereas traces of sulfur were observed after the Kesternich test. Therefore, it is concluded that the new compounds originated depend on the chemical elements added in the aging tests.

Author Contributions: Conceptualization, F.B.-M., F.S. and A.F.-G.; methodology, F.B.-M.; validation, F.B.-M.; formal analysis, F.B.-M.; investigation, F.B.-M.; resources, A.F.-G., F.S. and L.V.; data curation, F.B.-M. and A.G.-S.; writing—original draft preparation, F.B.-M.; writing—review and editing, A.F.-G., A.G.-S., F.S. and L.V.; supervision, A.F.-G., A.G.-S., F.S. and L.V.; project administration, A.F.-G., F.S. and L.V.; funding acquisition, A.F.-G., F.S. and L.V.

Conflicts of Interest: The authors declare no conflict of interest.

References

1. Tian, C.; Feng, G.; Li, S.; Xu, F. Scenario analysis on energy consumption and CO_2 emissions reduction potential in building heating sector at community level. *Sustainability* **2019**, *11*, 5392. [CrossRef]
2. Jäger-Waldau, A. Photovoltaics and renewable energies in Europe. *Renew. Sustain. Energy Rev.* **2007**, *11*, 1414–1437. [CrossRef]
3. Montoya, F.G.; Aguilera, M.J.; Manzano-Agugliaro, F. Renewable energy production in Spain: A review. *Renew. Sustain. Energy Rev.* **2014**, *33*, 509–531. [CrossRef]
4. Eldeen, H.; Aleem, A.; Andina, D.; Baldi, S.; Barone, M.; Bruno, M.; Daniel Carletti, D.; Carrillo, R.; Carvalho, M.; Souza, S. *Advances in Renewab Energies and Power Technologies*; Elsevier: Amsterdam, The Netherlands, 2018.
5. Mohtasham, J. Review article-renewable energies. *Energy Procedia* **2015**, *74*, 1289–1297. [CrossRef]
6. Solangi, K.H.; Islam, M.R.; Saidur, R.; Rahim, N.A.; Fayaz, H. A review on global solar energy policy. *Renew. Sustain. Energy Rev.* **2011**, *15*, 2149–2163. [CrossRef]
7. Cooke, P. Green governance and green clusters: Regional & national policies for the climate change challenge of Central & Eastern Europe. *J. Open Innov. Technol. Mark. Complex.* **2015**, *1*, 1–17.
8. Ummadisingu, A.; Soni, M.S. Concentrating solar power—Technology, potential and policy in India. *Renew. Sustain. Energy Rev.* **2011**, *15*, 5169–5175. [CrossRef]
9. International Energy Agency. *Renewables Information: Overview*; IEA Stat: Paris, France, 2017; p. 3.

10. García-Segura, A.; Fernández-García, A.; Buendía-Martínez, F.; Ariza, M.J.; Sutter, F.; Valenzuela, L. Durability studies of solar reflectors used in concentrating solar thermal technologies under corrosive sulfurous atmospheres. *Sustainability* **2018**, *10*, 3008. [CrossRef]

11. International Energy Agency. *Technology Roadmap—Solar Thermal Electricity*; IEA Stat: Paris, France, 2014.

12. Mills, D. Advances in solar thermal electricity technology. *Sol. Energy* **2004**, *76*, 19–31. [CrossRef]

13. García-Segura, A.; Fernández-García, A.; Ariza, M.J.; Valenzuela, L.; Sutter, F. Durability studies of solar reflectors: A review. *Renew. Sustain. Energy Rev.* **2016**, *62*, 453–467. [CrossRef]

14. Fernández-García, A.; Sutter, F.; Fernández-Reche, J.; Lüpfert, E. *The Performance of Concentrating Solar Power (CSP) Systems—Modelling Measurement and Assessment*; Elsevier: Amsterdam, The Netherlands, 2017; ISBN 978-0-08-100447-0.

15. Fernández-García, A.; Sutter, F.; Montecchi, M.; Sallaberry, F.; Heimsath, A.; Heras, C.; Le Baron, E.; Soum-Glaude, A. *Parameters and Method to Evaluate Reflectance Properties of Reflector Materials for Concentrating Solar Power Technology*; Oficial Reflectance Guideline Version 3.0; SolarPACES: Almería, Spain, 2018.

16. UNE 206016. *Reflector Panels for Concentrating Solar Technologies*; UNE: Madrid, Spain, 2018.

17. Montecchi, M.; Delord, C.; Raccurt, O.; Disdier, A.; Sallaberry, F.; García de Jalón, A.; Fernández-García, A.; Meyen, S.; Happich, C.; Heimsath, A.; et al. Hemispherical reflectance results of the SolarPACES reflectance round robin. *Energy Procedia* **2015**, *69*, 1904–1907. [CrossRef]

18. Fernández-García, A.; Sutter, F.; Heimsath, A.; Montecchi, M.; Sallaberry, F.; Peña-Lapuente, A.; Delord, C.; Martínez-Arcos, L.; Reche-Navarro, T.J.; Schmid, T.; et al. Simplified analysis of solar-weighted specular reflectance for mirrors with high specularity. *AIP Conf. Proc.* **2016**, *1734*, 130006.

19. Calvo, R.; Cantero, D. A new high sensitivity and low cost solution for the measurement of reflectance loss due to dust deposition in solar collectors. In Proceedings of the SolarPACES 2013, International Conference on Concentrating Solar Power and Chemical Energy Systems, Las Vegas, NV, USA, 17–20 September 2013.

20. Wolfertstetter, F.; Pottler, K.; Geuder, N.; Affolter, R.; Merrouni, A.A.; Mezrhab, A.; Pitz-Paal, R. Monitoring of mirror and sensor soling with TraCS for improved quality of ground based irradiance measurements. *Energy Procedia* **2014**, *49*, 2422–2432. [CrossRef]

21. Bouaddi, S.; Ihlal, A.; Fernández-García, A. Soiled CSP solar reflectors modelling using dynamic linear models. *Sol. Energy* **2015**, *122*, 847–863. [CrossRef]

22. Heimsath, A.; Nitz, P. The effect of soiling on the reflectance of solar reflector materials—Model for prediction of incidence angle dependent reflectance and attenuation due to dust deposition. *Sol. Energy Mater. Sol. Cells* **2019**, *195*, 258–268. [CrossRef]

23. Sutter, F.; Meyen, S.; Heller, P.; Pitz-Paal, R. Development of a spatially resolved reflectometer to monitor corrosion of solar reflectors. *Opt. Mater.* **2013**, *35*, 1600–1609. [CrossRef]

24. Sutter, F.; Meyen, S.; Fernández-García, A.; Heller, P. Spectral characterization of specular reflectance of solar mirrors. *Sol. Energy Mater. Sol. Cells* **2016**, *145*, 248–254. [CrossRef]

25. Montecchi, M. Upgrading of ENEA solar mirror qualification set-up. *Energy Procedia* **2014**, *49*, 2154–2161. [CrossRef]

26. Heimsath, A.; Schmid, T.; Nitz, P. Angle resolved specular reflectance measured with VLABS. *Energy Procedia* **2015**, *69*, 1895–1903. [CrossRef]

27. Sutter, F.; Fernández-García, A.; Heimsath, A.; Montecchi, M.; Pelayo, C. Advanced measurement techniques to characterize the near-specular reflectance of solar mirrors. *AIP Conf. Proc.* **2019**, *2126*, 110003.

28. ISO 9050. *Glass in Building, Determination of Light Transmittance, Solar Direct Transmittance, Total Solar Energy Transmittance, Ultraviolet Transmittance and Related Glazing Factors*; International Organization for Standardization: Geneva, Switzerland, 2003.

29. ASTM G173-03. *Standard Tables for Reference Solar Spectral Irradiances: Direct Normal and Hemispherical on 37° Tilted Surface*; ASTM: West Conshohocken, PA, USA, 2003.

30. Sutter, F.; Fernández-García, A.; Heller, P.; Anderson, K.; Wilson, G.; Schumücker, M.; Marvig, P. Durability testing of silvered-glass mirrors. *Energy Procedia* **2015**, *69*, 1568–1577. [CrossRef]

31. García-Segura, A.; Fernández-García, A.; Ariza, M.J.; Sutter, F.; Diamantino, T.; Martínez-Arcos, L.; Reche-Navarro, T.J.; Valenzuela, L. Influence of gaseous pollutants and their synergistic effects on the aging of reflector materials for concentrating solar thermal technologies. *Sol. Energy Mater. Sol. Cells* **2019**, *200*, 109955. [CrossRef]

32. García-Segura, A.; Fernández-García, A.; Ariza, M.J.; Sutter, F.; Valenzuela, L. Effects of reduced sulphur atmospheres on reflector materials for concentrating solar thermal applications. *Corros. Sci.* **2018**, *133*, 78–93. [CrossRef]

33. Kennedy, C.E.; Terwilliger, K. Optical durability of candidate solar reflectors. *J. Sol. Energy Eng.* **2005**, *127*, 262–269. [CrossRef]

34. Sutter, F.; Fernández-García, A.; Wette, J.; Heller, P. Comparison and evaluation of accelerated aging tests for reflectors. *Energy Procedia* **2014**, *49*, 1718–1727. [CrossRef]

35. Sansom, C.; Fernández-García, A.; King, P.; Sutter, F.; Garcia Segura, A. Reflectometer comparison for assessment of back-silvered glass solar mirrors. *Sol. Energy* **2017**, *155*, 496–505. [CrossRef]

36. Pettit, R.B. *Characterizing Solar Mirror Materials Using Portable Reflectometers*; Sandia National Laboratories: Albuquerque, NM, USA, 1982.

37. Fernández-García, A.; Sutter, F.; Martínez-Arcos, L.; Sansom, C.; Wolfertstetter, F.; Delord, C. Equipment and methods for measuring reflectance of concentrating solar reflector materials. *Sol. Energy Mater. Sol. Cells* **2017**, *167*, 28–52. [CrossRef]

38. Wiesinger, F.; Sutter, F.; Fernández-García, A.; Reinhold, J.; Pitz-Paal, R. Sand erosion on solar reflectors: Accelerated simulation and comparison with field data. *Sol. Energy Mater. Sol. Cells* **2016**, *145*, 303–3013. [CrossRef]

39. Bouaddi, S.; Ihlal, A.; Fernández-García, A. Comparative analysis of soiling of CSP mirror materials in arid zones. *Renew. Energy* **2017**, *101*, 437–449. [CrossRef]